

Anisotropic transport and quantum oscillations in the quasi-one-dimensional TaNiTe₅: Evidence for the nontrivial band topology

C. Q. Xu,^{1,2} Y. Liu,¹ P. G. Cai,¹ B. Li,^{3,4} W. H. Jiao,⁵ Y. L. Li,⁶ J. Y. Zhang,⁷ W. Zhou,⁷ B. Qian,⁷ X. F. Jiang,⁷ Z. X. Shi,⁸ R. Sankar,⁹ J. L. Zhang,¹⁰ F. Yang,¹¹ Zengwei Zhu,¹¹ P. K. Biswas,¹² Dong Qian,^{6,13} X. Ke,^{2,*} and Xiaofeng Xu^{1,†}

¹*Department of Applied Physics, Zhejiang University of Technology, Hangzhou 310023, China*

²*Department of Physics and Astronomy, Michigan State University, East Lansing, Michigan 48824-2320, USA*

³*New Energy Technology Engineering Laboratory of Jiangsu Province and School of Science, Nanjing University of Posts and Telecommunications, Nanjing 210023, China*

⁴*National Laboratory of Solid State Microstructures, Nanjing University, Nanjing 210093, China*

⁵*Department of Physics, Zhejiang University of Science and Technology, Hangzhou 310023, China*

⁶*Key Laboratory of Artificial Structures and Quantum Control (Ministry of Education), Shenyang National Laboratory for Materials Science, School of Physics and Astronomy, Shanghai Jiao Tong University, Shanghai 200240, China*

⁷*Department of Physics, Changshu Institute of Technology, Changshu 215500, China*

⁸*School of Physics and Key Laboratory of MEMS of the Ministry of Education, Southeast University, Nanjing 211189, China*

⁹*Institute of Physics, Academia Sinica, Nankang, Taipei, 11529, Taiwan*

¹⁰*High Magnetic Field Laboratory, Chinese Academy of Sciences, Hefei 230031, China*

¹¹*Wuhan National High Magnetic Field Center, School of Physics,*

Huazhong University of Science and Technology, Wuhan, 430074, China

¹²*ISIS Pulsed Neutron and Muon Source, STFC Rutherford Appleton Laboratory, Harwell Campus, Didcot, Oxfordshire OX11 0QX, United Kingdom*

¹³*Tsung-Dao Lee Institute, Shanghai Jiao Tong University, Shanghai 200240, China*

(Dated: June 17, 2020)

The past decade has witnessed the burgeoning discovery of a variety of topological states of matter with distinct nontrivial band topologies. Thus far, most of materials studied possess two-dimensional or three-dimensional electronic structures, with only a few exceptions that host quasi-one-dimensional (quasi-1D) topological electronic properties. Here we present the clear-cut evidence for Dirac fermions in the quasi-1D telluride TaNiTe₅. We show that its transport behaviors are highly anisotropic and we observe nontrivial Berry phases via the quantum oscillation measurements. The nontrivial band topology is further corroborated by first-principles calculations. Our results may help to guide the future quest for topological states in this new family of quasi-1D ternary chalcogenides.

I. INTRODUCTION

The interplay between dimensionality and electronic quantum states has been a fundamental theme of condensed matter physics for many decades. As a prominent example, it is well established that when electrons are spatially confined to a one-dimensional (1D) chain, interactions will drive the system into the 1D Luttinger-liquid regime with a characteristic feature of spin-charge separation^{1,2}. Recently, the exploration of solids with various nontrivial band topologies has become one of the heatedly pursued topics. Surprisingly, the vast majority of topological materials identified to date are electronically two-dimensional or three-dimensional in essence, with much fewer one-dimensional counterparts known to exist.

The quasi-1D topological material candidates reported thus far mainly involve the halogen compounds β -Bi₄X₄ (X = Br, I)³⁻⁵, α -Bi₄I₄^{5,6}, (TaSe₄)₂I⁷⁻⁹, the Weyl semimetal (Ta, Nb)IrTe₄¹⁰⁻¹³, and the theoretically proposed molybdenum chalcogenides A₂Mo₆X₆ (A = Alkali, In, Tl; X = chalcogen)¹⁴⁻¹⁶, etc. Among them, β -Bi₄I₄ has been experimentally verified as a weak topological insulator, i.e., the 3D stacking of 2D quantum

spin Hall (QSH) states, where topological surface states emerge only on the side surfaces but not on the top and bottom surfaces⁵. (TaSe₄)₂I was theoretically proposed and experimentally confirmed to be a type-III Weyl semimetal with larger chiral charges which can support four-fold helicoidal surface states with significantly long Fermi arcs⁸. TaIrTe₄ is a type-II Weyl semimetal with the minimum number of four Weyl points, which however are located above the Fermi level, making it challenging for real applications. The molybdenum chalcogenides A₂Mo₆X₆ were recently proposed to be a topological superconductor hosting cubic Dirac Fermions, which shows linear band crossing along one principal axis but cubic dispersion in the plane perpendicular to it. Nevertheless, due to the needle-shaped morphology of the as-grown samples, experimental validation of this type of topological states proves to be extremely challenging.

In this article, we report nontrivial topological electronic properties in the chain-containing ternary telluride TaNiTe₅ via comprehensive magnetization and transport measurements. The one-dimensional NiTe₂ chains are parallel to the crystallographic *a*-axis. As a result, this material exhibits highly anisotropic transport behaviors with ρ_a : ρ_b : $\rho_c \sim 1$: 16 : 7 at 320 K. The quantum os-

illations in both isothermal magnetization and magnetotransport measurements reveal light effective quasiparticle masses and nontrivial Berry phases. The nontrivial band topology is further supported by *ab initio* calculations. Our results establish that TaNiTe_5 represents a rare example of quasi-1D topological materials and is suitable for the study of interplay between dimensionality and band topology.

II. EXPERIMENTAL DETAILS

TaNiTe_5 single crystals were synthesized by the self-flux method. High-purity tantalum pieces, nickel shots and tellurium ingots were mixed with a molar ratio of 1 : 1 : 10 and sealed in an evacuated quartz tube. The quartz tube was then loaded into a box furnace and heated up to 1273 K quickly and kept at this temperature for 24 hours to ensure complete melting. The furnace was then slowly cooled down to 773 K with a rate of 5 K/h. After centrifugation at 773 K and fast-cooling to room temperature, shiny TaNiTe_5 single crystals in millimetre-long needles with an aspect ratio of $\sim 1:10$ (as shown in Fig. 1(c)) were obtained.

We checked the crystal quality and determined the structure of the as-grown samples using a four-circle X-ray diffractometer. The electrical resistivity and magneto-transport measurements were conducted using the Physical Property Measurement System (PPMS-9), and the magnetic susceptibility was measured using the Magnetic Property Measurement System (MPMS), both from Quantum Design. Magnetotransport measurements in the pulsed magnetic field up to 50 T were measured in Wuhan National High Magnetic Field Center, and Torque measurements were performed in the High Magnetic Field Laboratory in Hefei.

We also performed density functional theory (DFT) calculations by means of the full-potential linearized augmented plane wave method implemented in the WIEN2K package¹⁷ to obtain the electronic structure of TaNiTe_5 . The generalized gradient approximation (GGA) presented by Wu and Cohen¹⁸ was used for the exchange-correlation energy. This GGA is a nonempirical approximation that gives a significant improvement of calculations for lattice constants and crystal structures. Relativistic effects and spin-orbit coupling are included in all calculations. To further identify the topological properties, a tight-binding model based on maximally localized Wannier functions^{19,20} was constructed to reproduce the bulk band structure including spin-orbit coupling of Ta *d*, Ni *d* and Te *p* orbitals. Fermi surface was calculated on a dense $35 \times 35 \times 9$ *k*-point mesh in the full Brillouin zone. The extremal-orbit quantum oscillation frequencies of the calculated Fermi surfaces were analyzed using SKEAF (Supercell K-space Extremal Area Finder)²¹.

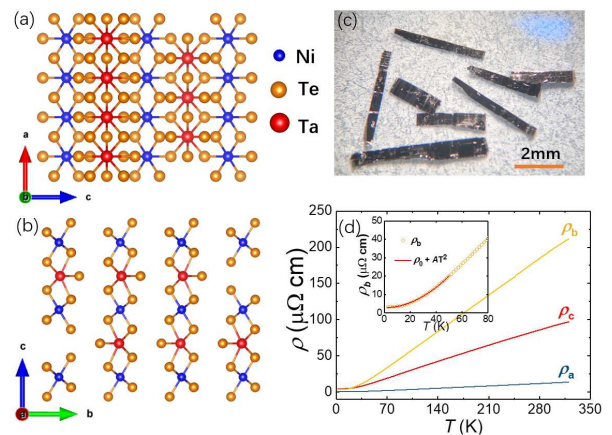


FIG. 1: Crystal structure of TaNiTe_5 viewed along the *b*-axis (a), and the *a*-axis (b). (c) The optical photo of some pieces of needle-like crystals. The longest direction is along the *a*-axis. (d) The temperature dependence of resistivity ρ_a , ρ_b , ρ_c with the current applied along the *a*, *b*, *c* axes, respectively. The inset shows the fit to the Fermi-liquid paradigm for a representative ρ_b .

III. RESULTS

TaNiTe_5 crystallizes in the orthorhombic space group (*Cmcm*, No. 63) with the lattice parameters of $a = 3.6674(7)\text{\AA}$, $b = 13.172(3)\text{\AA}$, $c = 15.142(3)\text{\AA}$, and $\alpha = \beta = \gamma = 90^\circ$ ²². As shown in Fig. 1, the structure consists of Ta bicapped trigonal prismatic chains which face-share with the adjacent Ni octahedral chains along the *a*-axis. Along the chain direction, two neighboring Ta atoms are connected via three Te atoms, and two neighboring Ni atoms are connected via two Te atoms²³. In contrast, the compound forms layer structure with large spacing between layers along the *b*-axis, as illustrated in Fig. 1(b). Fig. 1(c) shows the optic image of the crystals which exhibit a needle-like shape with cleavable flat surface perpendicular to the *b*-axis. Fig. 1(d) shows the temperature dependence of resistivity measured at zero field along three crystallographic axes. Evidently, this material exhibits quasi-1D transport behaviors with ρ_a : ρ_b : $\rho_c \sim 1 : 16 : 7$ at $T = 320$ K and $\sim 1 : 10 : 12$ at $T = 2$ K. Additionally, the resistivity closely follows linear-*T* dependence from 320 K to 50 K and crosses over to a Fermi liquid behavior with a quadratic *T* dependence below 50 K, as demonstrated in the inset of Fig. 1(d) for ρ_b (data of ρ_a and ρ_c show similar dependence and are not shown here), suggesting that the electron-electron scattering dominates in the low-*T* region.

Figure 2 displays the transverse magnetoresistance (MR) under different current and field-direction configurations. Interestingly, the MR of intrachain ρ_a shows notable difference compared to that of interchain ρ_b and ρ_c . Firstly, while ρ_a exhibits metallic behavior down to the lowest temperature even under a field of 9 T, a field-induced metal-to-insulator like transition was observed

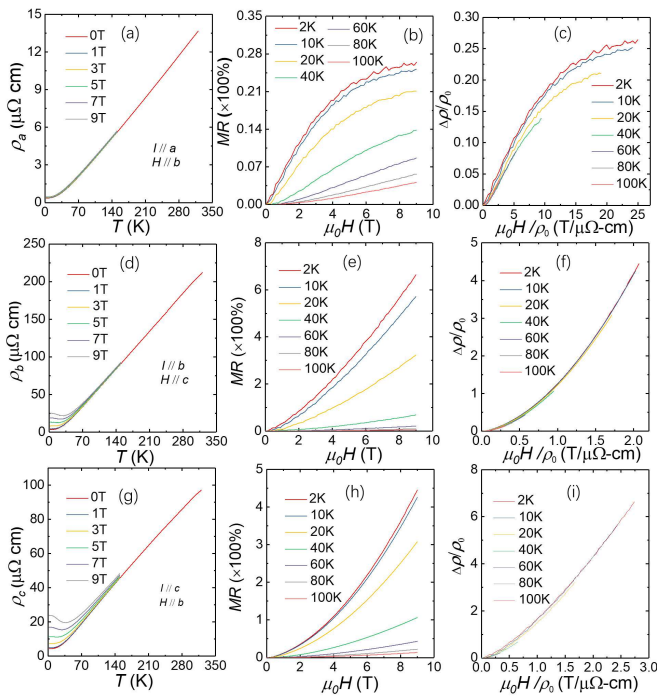


FIG. 2: (a-c) The temperature sweeps of ρ_a under various fields, the MR at fixed temperatures, and the Kohler's plot under the configuration of $I \parallel a$ and $H \parallel b$, respectively. (d-f) The same for $I \parallel b$ and $H \parallel c$. (g-i) The same for $I \parallel c$ and $H \parallel b$.

near $T = 30$ K for both ρ_b and ρ_c once $\mu_0 H \geq 7$ T, as presented in Fig. 2 (a, d, g). Secondly, in panels (b), (e) and (h), we plot the MR curves measured at fixed temperatures. As seen, MR is remarkably small for ρ_a and it tends to saturate with a low magnitude of $\sim 26\%$ at 2 K and 9 T. By contrast, ρ_b and ρ_c reaches a MR as high as 700% and 500% respectively without saturation at the same settings. These anisotropic transports signify the large anisotropic Fermi surfaces and the associated electron life time, reflecting its quasi-1D electronic structure. Finally, Fig. 2(c, f, i) show the Kohler's plots for these three configurations. It is evident that, for ρ_b and ρ_c , the Kohler's rule is well obeyed. However, for ρ_a , it is moderately violated, presumably due to the anisotropy in its carrier scattering time^{24,25}. Overall, these anisotropic magneto-transport behaviors also confirm the anisotropic electronic properties in this quasi-1D TaNiTe₅.

In order to gain more insights on the electronic structure of TaNiTe₅, we measured the quantum oscillations of its isothermal magnetization on single crystals with the magnetic field applied along two different crystallographic axes, i.e., $H \parallel a$ and $H \parallel b$. The insets of Fig. 3(a) and 3(b) present the isothermal magnetization $M(H)$ curves at $T = 2$ K with the magnetic field along the a and b axes, respectively, where de Haas-van Alphen oscillations (dHvA) are clearly observable. Remarkably, the susceptibility shows anisotropic, diamagnetic

signals over the whole field range with its anisotropic ratio (χ_b/χ_a) of ~ 5 at $\mu_0 H = 7$ T. Such anisotropy is commonly observed in layered materials and can be attributed to the anisotropic Lande- g factors^{26,27}. The oscillatory component becomes more visible after subtracting the diamagnetic background, as shown in Fig. 3(a) and 3(b). In Fig. 3(c) and 3(d), we plot the fast Fourier transform (FFT) analysis of ΔM . Interestingly, only two fundamental frequencies at $F_\alpha = 63$ T, $F_\beta = 251$ T are obtained for the magnetic field applied along the a axis; in contrast, four fundamental frequencies at $F_1 = 56$ T, $F_2 = 163$ T, $F_3 = 231$ T, $F_4 = 763$ T are clearly observed with the field along the b -axis. This again indicates that the Fermi surface morphology is indeed very anisotropic. Based on the Onsager relation $F = (\hbar/2\pi e)A_e$, we extracted the extremal Fermi-surface cross-sectional area A_e associated with each fundamental frequency within the Brillouin zone, as listed in Table I.

To proceed, we further performed the quantitative analysis of oscillatory data by the standard Lifshitz-Kosevich (LK) formula²⁸⁻³⁰.

$$\Delta M \propto -R_D R_T \sin\left\{2\pi\left[\frac{F}{B} + \left(\frac{1}{2} - \phi\right)\right]\right\} \quad (1)$$

where R_D is the Dingle damping term, R_T is the thermal damping factor. $R_D = \exp(2\pi^2 k_B T_D m^*/eB\hbar)$, and $R_T = \frac{2\pi^2 k_B T m^*/eB\hbar}{\sinh(2\pi^2 k_B T m^*/eB\hbar)}$, $\phi = \phi_B/2\pi - \delta$, where k_B is the Boltzmann constant, m^* is the effective electron mass, T_D is the Dingle temperature, ϕ_B is the Berry phase and δ is an additional phase shift depending on the dimensionality of the Fermi surfaces, i.e., $\delta = 0$ for 2D Fermi surfaces, and $\delta = \pm\frac{1}{8}$ for 3D Fermi surfaces ($-\frac{1}{8}$ for the electron-like, $+\frac{1}{8}$ for the hole-like, respectively). Therefore, one can determine the effective mass for each frequency by fitting the temperature dependence of the oscillatory components extracted from the FFT amplitude to R_T , as shown in Fig. 3(e) and 3(f). For $H \parallel a$, the effective electron masses corresponding to the two fundamental frequencies are $m_\alpha = 0.190m_0$, $m_\beta = 0.217m_0$ (m_0 is the free electron mass); for $H \parallel b$, the corresponding fits yield the effective masses of $m(F_1) = 0.169m_0$, $m(F_2) = 0.173m_0$, $m(F_3) = 0.180m_0$, $m(F_4) = 0.295m_0$. These small values of the effective mass for each frequency implies the presence of relativistic charge carriers. Besides, using the above fitted m , we can further fit $\Delta M(1/B)$ at a given temperature (e.g., $T = 2$ K) to the LK formula directly to obtain the Berry phase for each band. As shown in Fig. 3(g) and (h), the oscillations can be perfectly fitted using the above formula and the fitting procedure gives the Berry phase and the Dingle temperature for each band, as listed in Table I for completeness. As noted, some of Berry phases are close to π , suggesting the non-trivial fermions in TaNiTe₅.

In addition, we probed the Shubnikov-de Haas (SdH) oscillations of the magnetoresistance by extending the magnetic field up to 50 T. Here, we measured the inter-chain resistivity ρ_c instead of intra-chain ρ_a because ρ_c

TABLE I: Parameters obtained from the fitting of dHvA and SdH oscillations

| | (unit) | $H \parallel a$ | | $H \parallel b$ | | | | SdH | | | | |
|----------|-----------------------------|-----------------|------------|-----------------|------------|------------|------------|--------|--------|--------|----------|--------|
| | | dHvA | dHvA | F_1 | F_2 | F_3 | F_4 | F'_1 | F'_2 | F'_* | δ | F'_4 |
| F | (T) | 63 | 251 | 56 | 163 | 231 | 763 | 57 | 155 | 312 | 471 | 731 |
| A | (nm^{-2}) | 0.600 | 2.391 | 0.533 | 1.552 | 2.200 | 7.267 | 0.543 | 1.476 | 2.972 | 4.486 | 6.962 |
| m/m_e | | 0.190 | 0.217 | 0.169 | 0.173 | 0.180 | 0.295 | | 0.225 | 0.311 | 0.188 | 0.291 |
| T_D | (K) | 4.93 | 6.24 | 5.26 | 5.97 | 7.17 | 6.34 | | | | | |
| ϕ_B | ($\delta = -\frac{1}{8}$) | 1.497π | 1.972π | 1.502π | 0.870π | 1.212π | 0.730π | | | | | |
| | (0) | 1.247π | 1.722π | 1.252π | 0.620π | 0.962π | 0.480π | | | | | |
| | ($\delta = \frac{1}{8}$) | 0.997π | 1.472π | 1.002π | 0.370π | 0.712π | 0.230π | | | | | |

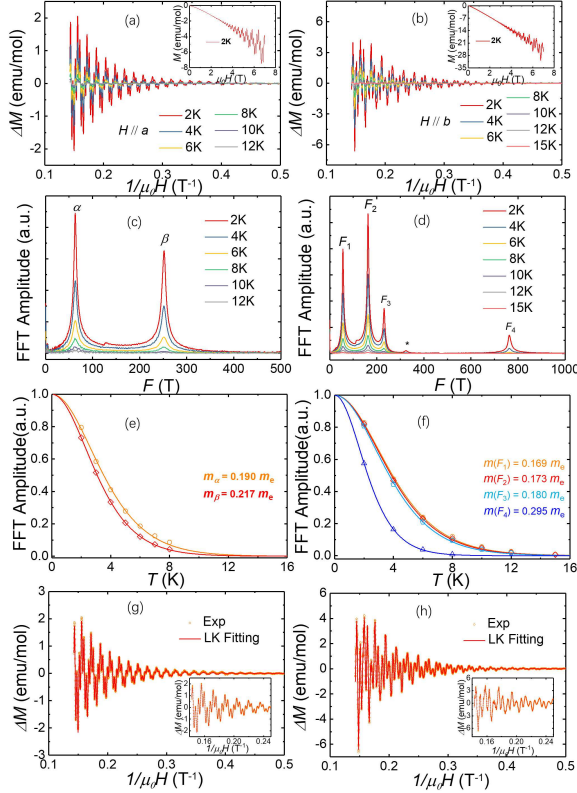


FIG. 3: Oscillatory components ΔM vs $\mu_0 H$ with $H \parallel a$ (a), $H \parallel b$ (b) at various temperatures. The insets of panel (a) and (b) are the raw data of $M - H$ at 2 K. (c) and (d) The FFT spectra of ΔM oscillations. (e) and (f) The temperature dependence of FFT amplitude. The solid lines are the LK fits for the effective mass. (g) and (h) The oscillatory components and the corresponding LK fits. The insets are the enlarged view to demonstrate the good fitting.

is the largest at low- T such that it gives the best signal-to-noise level. As shown in Fig. 4(a), MR reaches a magnitude of 4300% at $T = 2$ K, $H = 50$ T and the pronounced oscillations can be detected at high fields. After subtracting a smooth background, we extracted the oscillatory components, as illustrated in Fig. 4(b). From the FFT (Fig. 4(c)), we have derived five independent frequencies. Three of them (F'_1 , F'_2 , F'_4) are compar-

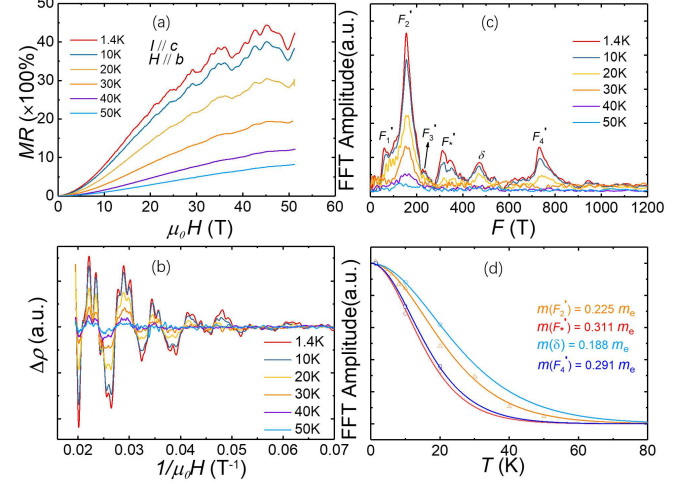


FIG. 4: (a) MR at different temperatures with $I \parallel c$, $H \parallel b$ up to 50 Tesla. (b) The oscillatory components at different temperatures. (c) FFT spectra of the SdH oscillations at different temperatures. (d) The temperature dependence of FFT amplitude and its fits. Note that we can not obtain $m(F'_1)$ due to its noisy signals.

ble with those from dHvA and the other two (F'_* and δ) seem to be the new frequencies. By employing the LK formula, the effective mass can be determined. Note that the m observed from SdH is larger than that from dHvA, especially for $m(F_2)$. This discrepancy between dHvA and SdH oscillations is often seen in low-dimensional materials such as the layered organic compounds and arises from the different mechanisms of dHvA and SdH oscillations³¹. It is known that SdH oscillations originate from the oscillating scattering rate and can thus be complicated by the detailed scattering procedures, imposed by lattice, impurity, inter/inner-Landau level scattering, etc.^{32,33}. In contrast, dHvA effect is caused directly by the oscillations of electrons' free energy.

To better understand the electronic properties of TaNiTe₅, we have performed DFT calculations to obtain its electronic structure. The calculated electronic band structure is shown in Fig. 5(a), with five bands crossing the Fermi level. In common with the quasi-1D Tl₂Mo₆Se₆ compound¹⁴, TaNiTe₅ also possesses the cu-

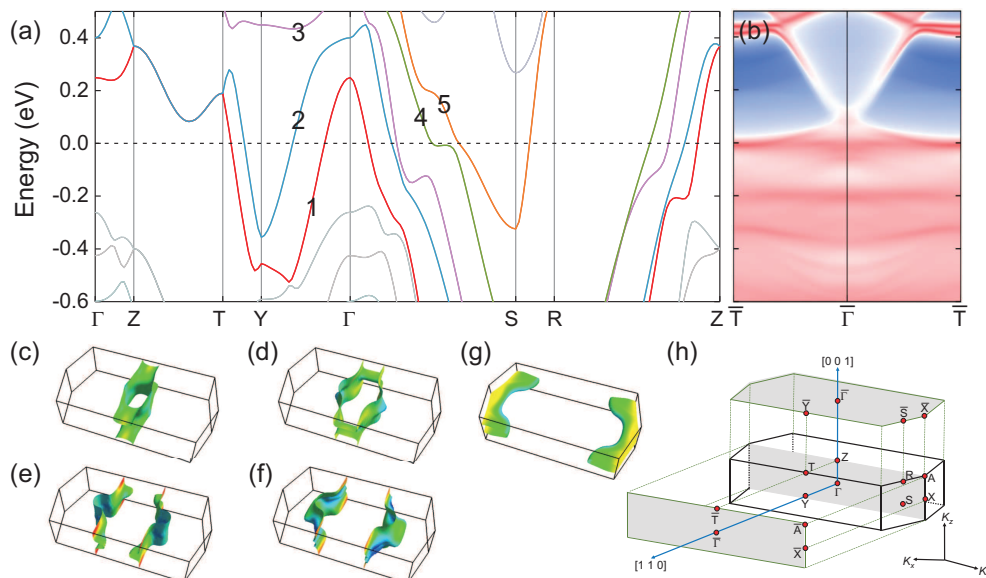


FIG. 5: (Color online) (a) Calculated band structure for bulk TaNiTe₅ with SOC included. The bands crossing the Fermi level are marked by different colors and labeled by numbers. (b) Surface state spectrum of TaNiTe₅ in the presence of SOC along high symmetry k -line $\bar{T} - \bar{\Gamma} - \bar{T}$. The bright red lines denote the surface states. (c-g) 3D Fermi surfaces from band 1 to band 5 as labeled in (a) with Fermi velocities shadowed. (h) The bulk and surface projected Brillouin zone (BZ) for primitive cell with high-symmetry points specified.

bic Dirac crossings in the $\Gamma - Z - T - Y$ direction, which have the quasi-linear band crossing along $\Gamma - Z$ and $T - Y$ but the cubic dispersions along $Z - T$. The cubic Dirac crossings are located at high symmetry points T $(-0.5, 0.5, 0.5)$ and Z $(0, 0, 0.5)$, as shown in Fig. 5(a). The Fermi surface analysis has been performed to determine the band type in the full Brillouin zone. It is found that Te-derived $5p$ orbital dominates around the Fermi level. The bulk Fermi surfaces with color-shadowed Fermi velocities are visualized in Fig. 5(c-g), which are comprised of five segments: band 1, band 2 are hole-dominated Fermi surfaces, and band 3, band 4 and band 5 are electron-dominated Fermi surfaces. The flatness of the Fermi surfaces indicates the quasi-1D feature expanding along the b direction in real space, which responds to $[110]$ direction in primitive reciprocal space. The calculated surface state spectrum along $\bar{T} - \bar{\Gamma} - \bar{T}$ is shown in Fig. 5(b). One can see significant bright red surface states along the slab direction forming Dirac-cone-like states at the slab center, which signify the topologically nontrivial characteristics of TaNiTe₅. The other piece of evidence for the topological non-triviality of TaNiTe₅ derives from its \mathbb{Z}_2 index. We calculated the \mathbb{Z}_2 topological number to further identify the topological properties. By using the Wilson loop technology²⁰, we obtained the \mathbb{Z}_2 topological number for TaNiTe₅, which is 1 for the $k_z = 0$ plane, and zeros for other planes. The resultant topological index is $(1, 000)$, whereby it makes a compelling case for the strong topological states in TaNiTe₅.

IV. CONCLUSION

In summary, we reported the synthesis of a new quasi-1D ternary telluride TaNiTe₅ and identified its possible topologically nontrivial states by means of electrical transport, quantum oscillations and the first-principles calculations. Specifically, its one-dimensionality is manifested in its large anisotropy in the resistivity and magnetoresistance and the susceptibility. The topological carriers are supported by nontrivial Berry phase extracted from the quantum oscillations, the Dirac band dispersions and the nontrivial \mathbb{Z}_2 index from the calculations. The findings presented in this work shall certainly invoke more theoretical study and the experimental investigations, such as (spin-polarized) ARPES and scanning tunnel microscopy, to probe the nontrivial bulk and surface states proposed in this study.

Acknowledgments

The authors would like to thank C. M. J. Andrew, Ali Bangura, Xin Lu for useful discussions. This work is sponsored by the National Natural Science Foundation of China (Grant No. 11974061, No. U1732162, No. 11521404, No. U1632272, No. U1832147, No. U1932217). W. H. J thanks the financial support from Zhejiang Provincial Natural Science Foundation of China (No. LY19A040002) and B. L. thanks NUPTSF (Grant No. NY219087, NY220038). R. S. acknowledges the financial support from the Ministry of Science and Tech-

nology in Taiwan under project number MOST-108-2112-M-001-049-MY2 and from Academia Sinica for the budget of AS-iMATE-109-13. X. Ke acknowledges the finan-

cial support from the start-ups at Michigan State University.

C. Q. Xu and Y. Liu contributed equally to this work.

-
- * Electronic address: kexiangl@msu.edu
 † Electronic address: xuxiaofeng@zjut.edu.cn
- ¹ S. Tomonaga, Remarks on Bloch's Method of Sound Waves applied to Many-Fermion Problems, *Prog. Theor. Phys.* **5**, 544 (1950).
 - ² J. M. Luttinger, An Exactly Soluble Model of a Many-Fermion System, *J. Math. Phys.* **4**, 1154 (1950).
 - ³ G. Autes, A. Isaeva, L. Moreschini, J. C. Johannsen, A. Pisoni, R. Mori, W. Zhang, T. G. Filatova, A. N. Kuznetsov, L. Forró, W. V. Broek, Y. Kim, K. S. Kim, A. Lanzara, J. D. Denlinger, E. Rotenberg, A. Bostwick, M. Grioni, and O. V. Yazyev, A novel quasi-one-dimensional topological insulator in bismuth iodide β -Bi₄I₄, *Nat. Mater.* **15**, 154(2016).
 - ⁴ C. C. Liu, J. J. Zhou, Y. Yao, and F. Zhang, Weak Topological Insulators and Composite Weyl Semimetals: β -Bi₄X₄(X = Br, I), *Phys. Rev. Lett.* **116**, 066801(2016).
 - ⁵ R. Noguchi, T. Takahashi, K. Kuroda, M. Ochi, T. Shirasawa, M. Sakano, C. Bareille, M. Nakayama, M. D. Watson, K. Yaji, A. Harasawa, H. Iwasawa, P. Dudin, T. K. Kim, M. Hoesch, V. Kandyba, A. Giampietri, A. Barinov, S. Shin, R. Arita, T. Sasagawa, and T. Kondo, A weak topological insulator state in quasi-one-dimensional bismuth iodide, *Nature* **566**, 518(2019).
 - ⁶ D. Y. Chen, D. S. Ma, Y. Li, Z. Z. Du, X. Xiong, Y. He, J. X. Duan, J. F. Han, D. Chen, W. D. Xiao, and Yugui Yao, *Phys. Rev. Mater.* **2**, 114408(2018).
 - ⁷ J. Gooth, B. Bradlyn, S. Honnali, C. Schindler, N. Kumar, J. Noky, Y. Qi, C. Shekhar, Y. Sun, Z. Wang, B. A. Bernevig, and C. Felser, Axionic charge-density wave in the Weyl semimetal (TaSe₄)₂I, *Nature* **575**, 315(2019).
 - ⁸ X. P. Li, K. Deng, B. Fu, Y. K. Li, D. S. Ma, J. F. Han, J. Zhou, S. Y. Zhou, Y. G. Yao, Type-III Weyl Semimetals and its Materialization, arXiv:1909.12178(2019).
 - ⁹ Y. Zhang, L. F. Lin, A. Moreo, S. Dong, E. Dagotto, First-principles study of the low-temperature charge density wave phase in the quasi-one-dimensional Weyl chiral compound ((TaSe₄)₂I), *Phys. Rev. B* **101**, 174106(2016).
 - ¹⁰ K. Koepf, D. Kasinathan, D. V. Efremov, S. Khim, S. Borisenko, B. Büchner, and Jeroen van den Brink, TaIrTe₄: A ternary type-II Weyl semimetal, *Phys. Rev. B* **93**, 201101(R)(2016)
 - ¹¹ E. Haubold, K. Koepf, D. Efremov, S. Khim, A. Fedorov, Y. Kushnirenko, J. van den Brink, S. Wurmehl, B. Büchner, T. K. Kim, M. Hoesch, K. Sumida, K. Taguchi, T. Yoshikawa, A. Kimura, T. Okuda, and S. V. Borisenko, Experimental realization of type-II Weyl state in noncentrosymmetric TaIrTe₄, *Phys. Rev. B* **95**, 241108(R)(2017)
 - ¹² W. Zhou, B. Li, C. Q. Xu, M. R. van Delft, Y. G. Chen, X. C. Fan, B. Q. N. E. Hussey, and Xiaofeng Xu, Nonsaturating Magnetoresistance and Nontrivial Band Topology of Type-II Weyl Semimetal NbIrTe₄, *Adv. Electron. Mater.* **5**, 1900250(2019).
 - ¹³ R. Schönemann, Y. C. Chiu, W. Zheng, V. L. Quito, S. Sur, G. T. McCandless, J. Y. Chan, and Luis Balicas, Bulk Fermi surface of the Weyl type-II semimetallic candidate NbIrTe₄, *Phys. Rev. B* **99**, 195128(2019).
 - ¹⁴ Z. Song, B. Li, C. Xu, S. Wu, B. Qian, T. Chen, P. K. Biswas, X. Xu, and J. Sun, Pressure engineering of the dirac fermions in quasi-one-dimensional Tl₂Mo₆Se₆, *J. Phys.: Condens. Matter* **32**, 215402 (2020).
 - ¹⁵ S. Mitra, A. P. Petrović, D. Salloum, P. Gougeon, M. Potel, J. X. Zhu, C. Panagopoulos, and E. E. M. Chia, Dimensional crossover in the quasi-one-dimensional superconductor Tl₂Mo₆Se₆, *Phys. Rev. B* **98**, 054507(2018).
 - ¹⁶ S. M. Huang, C. H. Hsu, S. Y. Xu, C. C. Lee, S. Y. Shiao, H. Lin, and A. Bansil, Topological superconductor in quasi-one-dimensional Tl_{2-x}Mo₆Se₆, *Phys. Rev. B* **97**, 014510(2018).
 - ¹⁷ K. Schwarz, P. Blaha, and G. K. H. Madsen, Electronic structure calculations of solids using the WIEN2k package for material sciences, *Comput. Phys. Commun.* **71**,147(1-2)(2002).
 - ¹⁸ Z. Wu, and R. E. Cohen, More accurate generalized gradient approximation for solids, *Phys. Rev. B* **73**, 235116 (2006).
 - ¹⁹ A. A. Mostofi, J. R. Yates, G. Pizzi, Y. S. Lee, I. Souza, D. Vanderbilt, N. Marzari, An updated version of wannier90 : A tool for obtaining maximally-localised Wannier functions. *Comput. Phys. Commun.* **185**, 2309(2014).
 - ²⁰ Q. S. Wu, S. N. Zhang, H. F. Song, M. Troyer, A. A. Soluyanov, WannierTools: An open-source software package for novel topological materials. *Comput. Phys. Commun.* **224**, 405(2017).
 - ²¹ P. M. C. Rourke, and S. R. Julian, Numerical extraction of de Haas-van Alphen frequencies from calculated band energies. *Comput. Phys. Commun.* **183**, 324 (2012).
 - ²² E. W. Liimatta, J. A. Ibers, Synthesis, structures, and conductivities of the new layered compounds Ta₃Pd₃Te₁₄ and TaNiTe₅, *J. Solid State Chem.* **78**, 7 (1989).
 - ²³ P. Alemany, and E. Canadell, Te...Te Interlayer Interactions, Te → Metal Electron Transfer and Electrical Conductivity in the MM'Te₅ Phases (M = Nb, M' = Ni, Pd; M = Ta, M' = Ni, Pt), *Eur. J. Inorg. Chem.* **1999**, 1701 (1999).
 - ²⁴ N. H. Jo, Y. Wu, L. L. Wang, P. P. Orth, S. S. Downing, S. Manni, D. Mou, D. D. Johnson, A. Kaminski, S. L. Bud'ko, and Paul C. Canfield, Extremely large magnetoresistance and Kohler's rule in PdSn₄: A complete study of thermodynamic, transport, and band-structure properties, *Phys. Rev. B* **96**, 165145 (2017).
 - ²⁵ N. Luo, G. H. Miley, Kohler's rule and relaxation rates in high-T_c superconductors, *Physica C* **371**, 259 (2002).
 - ²⁶ I. Terasaki, M. Hase, A. Maeda, K. Uchinokura, T. Kimura, K. Kishio, I. Tanaka, and H. Kojima, Doping effects on the anisotropic magnetic susceptibility in single-crystal La_{2-2x}Sr_xCuO₄, *Physica C* **193**, 365 (1992).
 - ²⁷ X. Xu, A. Carrington, A. I. Coldea, A. Enayati-Rad, A. Narduzzo, S. Horii, and N. E. Hussey, Dimensionality-driven spin-flop transition in quasi-one-dimensional PrBa₂Cu₄O₈, *Phys. Rev. B* **81**, 224435 (2010).

- ²⁸ I. M. Lifshits, and A. M. Kosevich, On the theory of magnetic susceptibility of metals at low temperatures, *Zh. Eksp. Teor. Fiz.* **29**, 730(1955).
- ²⁹ G. P. Mikitik, and Y. V. Sharlai, Manifestation of Berry's Phase in metal physics, *Phys. Rev. Lett.* **82**, 2147 (1999).
- ³⁰ Amit, R. K. Singh, N. Wadehra, S. Chakraverty, and Y. Singh, Type-II Dirac semimetal candidates ATe₂ (A = Pt, Pd): A de Haas-van Alphen study, *Phys. Rev. Mater.* **2**, 114202 (2018).
- ³¹ J. Hu, S.-Y. Xu, N. Ni, and Z. Mao, Transport of Topological Semimetals, *Annu. Rev. Mater. Res.* **49**, 207 (2019).
- ³² E. N. Adams, and T. D. Holstein, Quantum theory of transverse galvano-magnetic phenomena, *J. Phys. Chem. Sol.* **10**, 254 (1959).
- ³³ W. Gao, X. Zhu, J. Hue, S. Li, F. Zheng, H. Zhang, M. Wub, G. Zheng, N. Hao, P. Zhang, W. Ning, M. Tian, De Haas-van Alphen study on three-dimensional topological semimetal pyrite PtBi₂, *Sci. Bull.* **64**, 1496 (2019).